Probing Diverse Disulfur Ligands in the $Mo_2S_n^{-/0}$ (n = 4 ～ 8) Clusters: Structural Evolution and Chemical Bonding

ZHANG Xiao-Fei(张晓菲);LIU Xiu-Juan(刘秀娟);XU Ruo-Nan(徐若男);WU Ni(吴妮);HUANG Xin(黄昕);WANG Bin (王彬)

Department of Chemistry, Fuzhou University, Fuzhou 350116, *China*

ABSTRACT Density functional theory (DFT) and coupled cluster theory (CCSD(T)) calculations were employed to investigate the geometric and electronic structures of a range of dinuclear molybdenum sulfide clusters, $Mo_2S_n^-$ and Mo_2S_n (n = 4～8). The results showed that the sulfur atoms tended to occupy the terminal sites of the clusters continuously in the process of sequential sulfidation. After the oxidation state of Mo atoms reached the maximum of +6, diverse disulfur ligands emerged in the sulfur-rich $Mo_2S_n^{-/0}$ (n = 7, 8) clusters. The driving forces of removing a sulfur atom from different S ligands in $Mo_2S_n^{-/0}$ (n = 4～8) clusters, especially from those disulfur units, were evaluated. The corresponding order may provide insight into the pretreatment of fresh MoS_2 catalysts. Vertical detachment energies (VDEs) were predicted according to the Generalized Koopmans' theorem, and then the photoelectron spectra (PES) were simulated. Molecular orbital and spin density values were analyzed to elucidate the chemical bonding and the evolutionary behavior in the dinuclear molybdenum sulfide clusters.

Keywords: molybdenum sulfide; gas-phase cluster;density functional theory; supersulfido (S_2^-) ligand;simulated photoelectron spectrum, DOI: 10.14102/j.cnki.0254-5861.2011-1711

1 INTRODUCTION

Molybdenum sulfide has intensely caught people's eyes due to their wide applications in the fields of mechanical treatments, catalysts, energy materials and so forth[1–8]. In the case of catalysts, it is known that molybdenum sulfide can serve as a promising low-cost alternative to platinum or other noble metals catalyst in hydrogen evolution reaction (HER)[9–14]. Additionally, MoS_2-based catalysts have been widely used in the process of petroleum refining[15], including the hydrodesulfurization (HDS) and hydrodenitrogenation (HDN) reactions. Meanwhile, considerable attention has been paid to study the active sites in these catalysts[16–25]. It is normally accepted that the sulfur vacancies (or coordination unsaturated sites (CUS)) of MoS_2 are the key active centers[26, 27]. However, Besenbacher et al.[22] also put forward that the specific brim sites without sulfur vacancies are also responsible for the HDS activity. Furthermore, Vrubel et al.[11] showed that the reduced molybdenum sulfides containing the disulfide ligands appeared to be catalytically active. Several molybdenum complexes which contain various S_2 ligands have been synthesized recently, which were considered to be able to mimic the MoS_2 edge sites for the catalytic hydrogen generation[28–31]. Despite the progressive work, more detailed studies on the active sites of molybdenum sulfide catalysts are still required.

Previously, many studies have been focused on the synthesis and characterization of a variety of molybdenum polysulfido complexes and their precursors in the condensed phase, and various disulfide species were obtained in these complexes[28–30, 32–35]. Among them, the $[Mo_2S_7]^{2-}$ anion was found to possess a terminal S_2^{2-} ligand[32]. The $[Mo_2S_8]^{2-}$ was considered to own two terminal S_2^{2-} ligands[33]. The $[Mo_2S_{12}]^{2-}$ was reported to contain four terminal S_2^{2-} and two bridging S_2^{2-} ligands[30]. The $[Mo_3S_{13}]^{2-}$ was predicted to have three bridging S_2^{2-} and three terminal S_2^{2-} ligands[29]. These molybdenum complexes containing the persulfido (S_2^{2-}) ligands may lead to the corresponding complexes with supersulfido (S_2^{-}) ligands via futher electron transferation, but less is known about their supersulfido complexes[36–40]. As is known to all, gas-phase clusters can serve as effective molecular models gaining microcosmic understanding of the sophisticated surface structures and the catalytic processes at the molecular level[41–45]. Theoretical calculations have played an indispensable role in describing the accurate structure and properties of gas-phase clusters[46]. Over the past few years, considerable efforts have been devoted to studying the mono- and multi-nuclear molybdenum

sulfide gas-phase clusters[47–60]. Infrared spectra combined with DFT calculations of neutral mono-nuclear MS_n (M = Cr, Mo, W; n = 1～3) clusters have been studied by Andrews's group[59]. Joint experimental photoelectron spectra and theoretical investigations on a variety of mono- and multi-nuclear molybdenum sulfide clusters have also been reported by Gemming et al.[53, 57, 58]. Jiao et al. presented the structure and reactivity of Mo_3S_9 cluster which can be taken as a model for amorphous molybdenum sulfide MoS_3[54]. An *ab initio* study on the structural stability of Mo-S clusters and the size specific stoichiometries of magic clusters was reported by Murugan et al.[56], wherein Mo_2S_5 consisting of two bridging S and three terminal S atoms was expected to be the magic cluster. In spite of these efforts, the systematical theoretical investigations on the gas-phase molybdenum sulfide clusters are still required.

In our previous work[61, 62], we have reported a theoretical study on the mono-nuclear molybdenum sulfide clusters, $MoS_n^{-/0}$ (n = 1～6). To mimic the geometric and electronic properties of molybdenum sulfide surfaces and defects, larger Mo_xS_y clusters in size may be interesting. In the present work, extensive density functional theory (DFT) and coupled cluster theory (CCSD(T)) calculations were performed to elucidate the structural and electronic properties of a range of di-nuclear molybdenum sulfide clusters, $Mo_2S_n^-$ and Mo_2S_n (n = 4～8). The current study represents our continuous research interest in various clusters aiming at providing well-defined molecular models for bulk surfaces and catalysts[61–66]. According to our calculations, a behavior of structural evolution was found with the exception of neutral Mo_2S_8. The neutral Mo_2S_8 can be viewed as replacing two of the terminal S atoms in Mo_2S_6 by the same number of S_2 units. Interestingly, diverse disulfur ligands, including the supersulfido (S_2^-) ligands, emerged in sulfur-rich clusters $Mo_2S_n^{-/0}$ (n = 7, 8). It was found that the disulfur species may have a key impact on the catalytic activity[67–69]. Our calculations showed that the reduced reactions for removing one sulfur atom from the sulfur-rich clusters were spontaneous, whereas the reactions were nonspontaneous if the sulfur atom was removed from the sulfur-deficient clusters. The results suggested that the S_2 units may play an important role in removing the sulfur atoms from the edge sites of fresh MoS_2 catalysts.

2 COMPUTATIONAL METHODS

The calculation details for this study are similar to our earlier studies on mono-nuclear molybdenum sulfide clusters, $MoS_n^{-/0}$ (n = 1∼6)[61, 62]. Density functional theory (DFT) calculations employing the B3LYP hybrid functional[70–72] were carried out using Gaussian 03 program[73]. B3LYP was widely used in quantum chemistry[74]. Furthermore, B3LYP had been applied in the other Mo-S systems, which showed good agreement with the experimental data[51, 54, 59]. Additionally, B3LYP also gave reasonably good results which were compared to the available experimental data in our previous work[61–66]. As discussed below, we used the results with B3LYP functional for further discussion. A host of initial structures considering different spin states and geometric symmetry were evaluated, and the search for the most stable structures was first performed using the triple-ζ valence plus polarization (def2-TZVP) basis set[75–77] and the corresponding Stuttgart effective core potential for Mo[78] (denoted as L-BS hereafter). Then the selected low-lying isomers (ΔE < 0.50 eV) were further re-optimized at the B3LYP level with the larger basis sets, i.e., the Stuttgart relativistic small core basis set and efficient core potential[78, 79] augmented with two *f*-type and one *g*-type polarization functions ($\zeta(f)$ = 0.338, 1.223; $\zeta(g)$ = 0.744) for molybdenum[80] and the aug-cc-pvtz basis set for sulfur and hydrogen[81–83] (denoted as H-BS hereafter). Scalar relativistic effects were taken into account via the quasi-relativistic pseudo-potentials. Vibrational frequency was calculated at the same level of theory to confirm that the reported minima have no imaginary frequency. The relative stabilities of several energetically close-lying isomers (ΔE < 0.40 eV) were further distinguished with the help of higher-level CCSD(T)[84–88] single point calculations with the H-BS basis sets at the B3LYP optimized geometries. Vertical electron detachment energies (VDEs) were calculated on the basis of the generalized Koopmans' theorem[89] which had been described detailedly in our previous studies[61–66]. All DFT calculations were performed using the Gaussian 03 software package. The CCSD(T) calculations were performed with the MOLPRO 2010.1 package[90]. The frontier molecular orbitals were visualized using the VMD software[91].

3 THEORETICAL RESULTS

The optimized geometries for the ground-state and selected energetically low-lying isomers of $Mo_2S_n^-$ and Mo_2S_n (n = 4∼8) at the B3LYP/H-BS level of theory are displayed in Figs. 1∼5. Their relative energies

including those isomers within 0.40 eV at the B3LYP/H-BS level together with the results of single-point CCSD(T) calculations are collected in Table 1. Alternative optimized results at the B3LYP/L-BS level for $Mo_2S_n^{-/0}$ (n = 4∼8) are given in the Supporting Information (Figs. S1∼S5).

3. 1 Sulfur-deficient clusters: Mo_2S_n and $Mo_2S_n^-$ (n = 4, 5)

Previously, the tribridged structure with three bridging S atoms and the dibridged structure with two bridging S atoms and one terminal S atom were reported to be the possible ground states of the Mo_2S_3 cluster[56, 58]. To search for the ground states of $Mo_2S_4^{-/0}$, a host of initial structures were taken into consideration, including the above mentioned dibridged and tribridged strucutres. Based on the calculations, a nonplanar dibridged structure (C_s, $^3A''$) is shown to be the lowest-energy structure of Mo_2S_4 (Fig. 1a). Another triplet state ($^3A_2$) with higher symmetry C_{2v} is only 0.04 eV (Fig. 1b) higher in energy. The corresponding quintet state ($^5B_1$) with C_{2v} symmetry is located to be 0.15 eV (Fig. 1c) higher in energy. The quintet state (^5B_g) with C_{2h} symmetry is 0.21 eV (Fig. 1d) higher in energy. The difference between these two quintet states is that two terminal S atoms in the former show a *syn* relationship, whereas the latter has a *anti* configuration. In addition, the triplet state (C_s, $^3A''$) with the *anti* configuration is 0.30 eV (Fig. 1e) higher in energy. It seems that the *syn* configuration is more stable than the *anti* configuration. The previous studies[47, 48, 56, 58] have also supported the dibridged structure which has the *syn* configuration to be the ground state of Mo_2S_4. For the anionic species, the dibridged structure (C_{2v}, $^4B_1$) with *syn* configuration is found to be the lowest-energy structure of $Mo_2S_4^-$ (Fig. 1g). Another two dibridged isomers, C_{2h} (^4B_g) and C_{2v} ($^2B_1$), are located to be 0.18 eV (Fig. 1h) and 0.34 eV (Fig. 1i) higher in energy, respectively. Other optimized isomers for both the neutral and the anion are much higher in energy and thus not listed in the current paper. More optimized structures at the B3LYP/L-BS level are available in the Supporting Information (Fig. S1).

Starting from the ground states of $Mo_2S_4^{-/0}$ clusters, extensive structural searches revealed the singlet (C_s, $^1A'$) to be the ground state of Mo_2S_5 (Fig. 2a). It can be viewed as adding a terminal S atom to the dibridged Mo_2S_4. The previous studies by Murugan et al.[56] and Gemming et al.[58] also supported our results. The corresponding triplet state (C_s, $^3A'$) is 0.17 eV (Fig. 2b) higher in energy. For the anionic $Mo_2S_5^-$, the ground state (Fig. 2c) is found to be a doublet state (C_s, $^2A'$), whose geometry is similar to that of the neutral ground state. A quartet (C_{2v}, $^4A_2$) is located to be 0.22 eV (Fig. 2d) above the ground state.

3. 2 Stoichiometric clusters: Mo_2S_6 and $Mo_2S_6^-$

The ground state of Mo_2S_6 is identified to have C_{2v} ($^1A_1$) symmetry (Fig. 3a). It can be deemed as adding a terminal S atom to the Mo_2S_5 ground state. Each Mo atom in Mo_2S_6 is tetra-coordinated with two terminal S atoms and two bridging S atoms. This result is in consistent with the previous study by Gemming et al.[58]. It should be mentioned that the isomer with a terminal S_2 unit was expected to be the most stable structure of Mo_2S_6 by Murugan et al.[56]. But this isomer is less stable (> 0.50 eV) than the structure in Fig. 3a according to our calculation (Fig. S3). For the anionic $Mo_2S_6^-$, an open-shell (^2A_g) structure with D_{2h} symmetry is found to be the ground state (Fig. 3b).

3. 3 Sulfur-rich clusters: Mo_2S_n and $Mo_2S_n^-$ (n = 7, 8)

To our knowledge, no other computational studies have been reported for the gas-phase $Mo_2S_7^{-/0}$ and $Mo_2S_8^{-/0}$ clusters. On the basis of our calculations on $Mo_2S_6^{-/0}$, various initial configurations with different spin multiplicities were studied in search of the ground states of $Mo_2S_7^{-/0}$. As shown in Fig. 4a, the lowest-energy structure of Mo_2S_7 is predicated to be closed-shell (^1A) with C_2 symmetry wherein a bridging S_2 unit appears. It can be regarded as replacing one of the bridging S atoms in Mo_2S_6 by a bridging S_2 unit. The S–S bond length of the S_2 unit in Mo_2S_7 (Fig. 4a) is 2.086 Å. A triplet state (C_s, $^3A''$) with a terminal S_2 unit (Fig. 4b) is located 0.26 eV above the ground state. However, this structure becomes the ground state of the $Mo_2S_7^-$ anion (Fig. 4d), whereas the structure with a bridging S_2 unit (Fig. 4e) is 0.39 eV higher in energy. The $Mo_2S_7^-$ ground state can be seen as replacing one of the terminal S atoms in $Mo_2S_6^-$ by a terminal S_2 unit. The terminal S_2 ligand in $Mo_2S_7^-$ (Fig. 4d) is attached in a side-on fashion, and the corresponding S–S bond length is 2.097 Å.

In the case of $Mo_2S_8^{-/0}$, we found several close-lying isomers of $Mo_2S_8^{-/0}$ near the lowest-energy structure. As shown in Fig. 5a, the ground state of Mo_2S_8 is found to be $^3B_2$ state with C_{2v} symmetry, which can be viewed as replacing two terminal S atoms in Mo_2S_6 by two terminal S_2 units in a *syn* configuration. The S–S bond lengths in the S_2 units are calculated to be 1.999 Å, and the Mo–S_2 bond lengths are 2.468 Å. Another triplet state (C_{2h}, ^3B_u) which also has two terminal S_2 ligands but in a *anti* configuration is 0.20 eV (Fig. 5b) above the ground state. In addition, the isomer which can be seen as replacing the remaining bridging S in Mo_2S_7 by a bridging S_2 unit is much higher in energy (> 0.5 eV; Fig. S5). For the anion, the most stable structure of $Mo_2S_8^-$ (Fig. 5c) is a doublet state with C_{2v} symmetry, in which two terminal S_2 ligands are in a

syn relationship as in the case of the neutral. The *anti* isomer (C_{2h}, ^2B_g) is shown to be 0.06 eV (Fig. 5d) higher in energy. Additionally, the isomer which contains a terminal S_3 ligand is 0.11 eV (Fig. 5e) higher in energy. Similar with the results of $Mo_2S_4^{-/0}$, the calculations showed that the *syn* configuration seems to be more stable than the *anti* configuration for $Mo_2S_8^{-/0}$.

3. 4 CCSD(T) single-point calculations for low-lying structures

The low-lying isomers of Mo_2S_n (n = 4∼8) and their anion species (within 0.40 eV at the B3LYP/H-BS level) were further evaluated using higher level single point CCSD(T) calculations at the B3LYP geometries. The relative energies of single point CCSD(T) calculations are summarized in Table 1. As a whole, the results of single point CCSD(T) calculations are in good line with that of DFT/B3LYP calculations, except for the neutral Mo_2S_4. According to the CCSD(T) calculations (Table 1), the second lowest-energy isomer (C_{2v}, $^3A_2$; Fig. 1b) of Mo_2S_4 seems more stable than the isomer (C_s, ^3A") shown in Fig. 1a. Although these two isomers are close in erengy (0.07 eV) at the CCSD(T) level, they are likewise similar in their geometries and electronic structures. Herein, the Mo_2S_4 (C_{2v}, $^3A_2$) shown in Fig. 1b is tentatively considered to be the ground state.

4 DISSCUSION

4. 1 Interpretation of the simulated spectra and molecular orbital analyses

The experimental PES spectra which can be used as an electronic “fingerprint” of a given cluster could provide valuable electronic information. On the basis of generalized Koopmans’ theorem, the vertical detachment energies (VDEs) for the identified $Mo_2S_n^-$ (n = 4∼8) anionic ground states and the selected low-lying isomers (ΔE < 0.40 eV) were calculated (Table 2). The introduction to the principles of PES spectra simulation may be found in the early references[92]. This simulation method has been extensively used in a number of previous studies[61, 66, 94–96] and show good agreement with the experimental spectra. The simulated PES spectra are presented in Fig. 12. The first vertical detachment energy (VDE_{1st}) trend as a function of S content (n) in $Mo_2S_n^-$ (n = 4∼8) is displayed in Fig. 13.

4. 1. 1 Mo_2S_4 and $Mo_2S_4^-$

The frontier orbitals of Mo_2S_4 and $Mo_2S_4^-$ are illustrated in Fig. 6. As mentioned above, the Mo_2S_4 (C_{2v},

$^3A_2$) as shown in Fig. 1b is considered to be the ground state using the CCSD(T) single-point calculations. Its valence electronic configuration is $(18a_1)^2(10b_1)^2(6a_2)^1(19a_1)^1$. Addition of an electron into the empty antibonding orbital 13b$_2$ of the neutral (Fig. 6a) would lead to the anionic ground state $Mo_2S_4^-$ (C_{2v}, $^4B_1$) as shown in Fig. 1g. The corresponding valence electronic configuration is $(10b_1)^2(18a_1)^2(6a_2)^1(13b_2)^1(19a_1)^1$. Accordingly, the Mo–Mo distances increase from 2.616 to 2.760 Å, as shown in Fig. 1b and 1g. The VDE$_{1st}$ upon photodetachment from the singly occupied bonding orbital $(19a_1)^1$, which is mainly characterized by a Mo 4*d* orbital, is predicted to be 3.39 eV. The fully occupied 10b_1 MO and below are mainly of S 3*p* character. Other calculated VDEs from 13b_2 and below are presented in Table 2.

4. 1. 2 Mo_2S_5 and $Mo_2S_5^-$

The ground state of neutral Mo_2S_5 (C_s, $^1A'$) is predicated to be closed-shell species (Fig. 2a). The valence electronic configuration of Mo_2S_5 is $(36a')^2(37a')^2$. Addition of an electron into the empty bonding orbital 38a' of the neutral (Fig. 7a) would lead to the anionic ground state $Mo_2S_5^-$ (C_s, $^2A'$; Fig. 2c) with a valence electronic configuration of $(36a')^2(37a')^2(38a')^1$. As shown in Fig. 7b, the singly occupied molecular orbital (SOMO) 38*a*' and the fully occupied orbital 36a' primarily correspond to the Mo 4*d* orbitals, and the orbital 37*a*' is characterized by S 3*p* feature. The first detachment channel for $Mo_2S_5^-$ is derived from the removal of the SOMO 38*a*', for which the calculated VDE is 3.76 eV.

4. 1. 3 Mo_2S_6 and $Mo_2S_6^-$

The neutral Mo_2S_6 (Fig. 3a) is stoichiometric in which each Mo achieves its highest oxidation state Mo^{6+}. In other words, all of six valence electrons of Mo [$4d^55s^1$] are used to form bonds with the S atoms. The valence electronic configuration of the neutral Mo_2S_6 (C_{2v}, $^1A_1$) cluster is $(24a_1)^2(12b_1)^2(19b_2)^2$. The highest occupied molecular orbital (HOMO) 19b_2 and lowest unoccupied molecular orbital (LUMO) 25a_1 are depicted in Fig. 8a. All MOs from HOMO and below are S 3*p*-based orbitals, and the LUMO is primarily featured by the Mo 4*d* orbital. When one extra electron is added to the neutral Mo_2S_6, the ground state of $Mo_2S_6^-$ (Fig. 3b) would still maintain the skeleton of neutral (Fig. 3a) but the rhombus Mo_2S_2 unit in the neutral is distorted relative to the anion. The valence electronic configuration of $Mo_2S_6^-$ (D_{2h}, ^2A_g) is $(4b_{3g})^2(10b_{2u})^2(15a_g)^1$. In this D_{2h} structure, the extra electron delocalized on the two Mo atoms, as is evidenced from its SOMO 15a_g (Fig. 8b). The photodetachment from SOMO 15a_g yields the VDE$_{1st}$ with a calculated value of 4.51 eV. The

remaining calculated VDEs from $10b_{2u}$ and below are presented in Table 2.

4. 1. 4 Mo_2S_7 and $Mo_2S_7^-$

For the sulfur-rich species Mo_2S_7, the structure with a S_2 unit in the bridging fashion is predicated to be the neutral ground state (Fig. 4a), for which the valence electronic configuration is $(35a)^2(33b)^2(36a)^2(34b)^2$. All the MOs are featured by 3*p* orbital of S atom (Fig. 9a). The ground state of anion $Mo_2S_7^-$ (C_1, ^2A) is predicted to be open-shell with a terminal S_2 group (Fig. 4d). The valence electronic configuration of this anion is $(65a)^2(66a)^2(67a)^2(68a)^1(69a)^2(70a)^2(71a)^2$. The calculated S–S bond length in this S_2 group is 2.097 Å, which is similar with the free S_2^{2-} ($^1\Sigma_g^+$) dianion (2.180 Å calculated at the same level). The two fully occupied orbitals 71*a* and 65*a* correspond to the π^* orbitals of S_2 group (Fig. 9b). Hence, the $Mo_2S_7^-$ C_1 (^1A) can be considered as the addition of a S_2^{2-} unit to the cationic $Mo_2S_5^+$. Photodetachment from the fully occupied orbital 71*a* yields the first PES band with the calculated VDEs of 4.32 eV (α) and 4.26 eV (β). The detachment origining from the singly occupid orbital $68a_1$ requires a higher energy (5.00 eV).

4. 1. 5 Mo_2S_8 and $Mo_2S_8^-$

The frontier MOs of Mo_2S_8 and $Mo_2S_8^-$ are illustrated in Fig. 10. The ground state of Mo_2S_8 is found to be $^3B_2$ state with C_{2v} symmetry (Fig. 5a). The valence electronic configuration for the neutral species is $(16b_1)^2(26a_1)^2(17b_1)^1(13a_2)^1(18b_1)^2(27a_1)^2$. The corresponding frontier MO pictures are shown in Fig. 10a, in which two singly occupied orbitals $13a_2$, $17b_1$ and two doubly occupied orbitals $16b_1$ and $18b_1$ correspond to the π^* orbitals of two bound S_2 units in Mo_2S_8 (C_{2v}, $^3B_2$). Furthermore, the S–S bond length of the S_2 moiety (1.999 Å in Fig. 5a) is very close to that of free S_2^- ($^2\Pi_g$) anion (2.029 Å calculated at the same level). The spin density analyses further certify that two unpaired electrons are separately located on two S_2 units (Fig. 11a). Therefore, the Mo_2S_8 (C_{2v}, $^3B_2$) may be viewed as two S_2^- units adhered to the cationic $Mo_2S_4^{2+}$. For the anionic species, the valence electronic configuration is $(16b_1)^2(26a_1)^2(17b_1)^2(27a_1)^2(13a_2)^2(18b_1)^1$. As shown in Fig. 10b, the singly occupied MO $18b_1$ and three doubly occupied MOs $13a_2$, $17b_1$ and $16b_1$ correspond to the π^* orbitals of the S–S moieties. The bond length of S_2 unit (2.055 Å) is between that of the bound S_2^- and S_2^{2-} anions (1.999 Å in Fig. 5a and 2.097 Å in Fig. 4d, respectively). The spin density analyses show that an unpaired electron is equiprobably shared by two terminal S_2 groups (Fig. 11b). Therefore, the $Mo_2S_8^-$ (C_{2v}, $^2B_1$; Fig. 5c) cluster can be described as a resonance hybrid of two equivalent C_s structures with both S_2^- and S_2^{2-}

units. As shown in Table 2 and Fig. 12e, photodetachment from the fully occupied 13a_2 orbital (Fig. 10b) of $Mo_2S_8^-$ yields the first PES band with the calculated VDE_{1st} of 3.58 eV (β).

4. 2 Structural evolution of $Mo_2S_n^{-/0}$ (n = 4∼8) clusters

As noted above, a series of thiomolybdate dianion $Mo_2S_n^{2-}$ (n = 6∼9) have been prepared and characterized in condensed phase[33]. It was pointed out that six homologues $[Mo_2S_n]^{2-}$ (n = 6∼12) dianions may be obtained from any other by either adding sulfur or removing sulfur by triphenylphosphine (Ph_3P)[32]. In our paper, similar structural evolutions are found for the gas-phase $Mo_2S_n^{-/0}$ (n = 4∼8) clusters.

It is worth to mention that Mo_2S_6 showed the highest stability among a series of Mo_2S_y clusters by Gemming et al.[58]. They indicated that the structure of Mo_2S_6 may be used as a motif of larger Mo_xS_y clusters or the bulk MoS_3 phase. In our calculations, the ground state of Mo_2S_6 (C_{2v}, $^1A_1$; Fig. 3a) possesses four Mo=S double bonds and four Mo−S single bonds, in which each Mo atom has reached its highest oxidation state of +6.

For the neutrals, with the increasing sulfur content, the formal oxidation state of molybdenum increases until reaching its highest oxidation state of +6. Meanwhile, the sulfur atoms occupy the terminal sites in Mo_2S_n clusters (n = 4∼6) successively. After both Mo atoms get the highest oxidation state, the disulfur units (i.e., S_2) begin to emerge. Namely, one of the bridging S atoms in Mo_2S_6 is replaced by a bridging S_2 unit for the Mo_2S_7 cluster. Then for the Mo_2S_8 cluster, two of the terminal S atoms in Mo_2S_6 are replaced by the same number of terminal S_2 ligands.

Similar evolutionary regularities are also found for the anionic $Mo_2S_n^-$ (n = 4∼6) clusters. They preserve the structural skeleton of their neutral counterpart. In $Mo_2S_7^-$ cluster, one of the terminal S atoms in $Mo_2S_6^-$ is replaced by a terminal S_2 ligand. Subsequently in the $Mo_2S_8^-$ cluster, two terminal S atoms in $Mo_2S_6^-$ are replaced by the same number of terminal S_2 ligands. Furthermore, based on the relative stability of $Mo_2S_4^{-/0}$ and $Mo_2S_8^{-/0}$ (Figs. 1 and 5), it seems that the *syn* configuration is more stable than the *anti* one.

4. 3 Trend of VDE_{1st} as the function of S content in $Mo_2S_n^-$ (n = 4∼8)

Fig. 13 depicts the trend of calculated VDE_{1st} as a function of S content in the $Mo_2S_n^-$ clusters. The trend of VDE_{1st} can be qualitatively understood from the frontier MO analysis (Figs. 6∼10). The VDE_{1st} increases nearly linearly as a function of sulfur content (n = 4∼6), clearly showing a behavior of sequential sulfidation

of Mo_2 dimer. The valence electrons of molybdenum ($4d^5 5s^1$) are sequentially transferred to the added S atoms, along with the number of Mo 4*d*-based orbitals decrease (Figs. 6∼8). Interestingly, the VDE_{1st} suddenly begins to reduce after that. The reason why the VDE_{1st} starts to decrease can also be comprehended from the frontier MO analysis as shown in Figs. 9 and 10. When *n* reaches 7 (i.e., $Mo_2S_7^-$), the detachment is origining from the fully occupied π^* orbitals (71a) of a S_2 unit, leading to the decrease of VDE_{1st} (from 4.51 to 4.26 eV). When *n* is equal to eight (i.e., $Mo_2S_8^-$), we found the $VDEs_{1st}$ corresponds to the detachment from the singly occupied π^* orbitals ($18b_1$) of two S_2 moieties. The further decreasement of VDE_{1st} from 4.26 to 3.58 eV may be a consequence of distribution of an unpaired electron over the π^* orbitals of two S_2 groups.

4. 4 Reduction reaction of H_2 on the $Mo_2S_n^{-/0}$ (*n* = 4∼8) clusters

Afanasiev *et al*.[67, 68] showed that the S_2^{2-} species located at the edges of fresh MoS_2 catalysts play a key part for the catalytic activity. Recently, Karunadasa and co-workers[28] have reported the synthesis of a side-on bound Mo^{IV}-disulfide complex, which could mimic the MoS_2 edge sites for the catalytic hydrogen generation. It is interesting to note that diverse S_2 units are found in the sulfur-rich clusters $Mo_2S_n^{-/0}$ (*n* = 7, 8) in our work.

The MoS_2 catalysts are usually used in the gaseous environment of H_2/H_2S at raised temperature. The experiment pointed out that the kinetics of S_2 group interaction with hydrogen could be promoted by the reactant H_2 and hindered by the product H_2S[67]. Thus, we proposed the reaction (eq. 1) removing a sulfur atom from $Mo_2S_n^{-/0}$ (*n* = 4∼8) clusters. The driving force can be estimated by the negative values of Gibbs free energy differences (ΔG) of this reaction, which are obtained by the following equation (eq. 2) and summarized in Table 3.

$$Mo_2S_n^{-/0} + H_2 \rightleftharpoons Mo_2S_{n-1}^{-/0} + H_2S \quad (1)$$

$$\Delta G = G(Mo_2S_{n-1}^{-/0}) + G(H_2S) - G(Mo_2S_n^{-/0}) - G(H_2) \quad (2)$$

In light of the values of ΔG, the driving forces of the proposed reactions increase as a function of *n*. For the proposed reaction (Eq. 1; *n* = 5, 6), the sulfur is removed from the terminal S of $Mo_2S_5^{-/0}$ and $Mo_2S_6^{-/0}$. The corresponding values of ΔG (Table 3) are positive (*Reactant-favored*). After both of the Mo atoms reach their maximum oxidation state of +6, the S_2 units begin to emerge. The energy costs (ΔG) of sulfur atom losing from various S_2 units start to be negative (*Product-favored*). So, for the sulfur-rich clusters $Mo_2S_n^{-/0}$ (*n* = 7, 8),

regardless of the kinetic factor, the proposed reactions (Eq. 2) may be energetically (thermodynamically) favored. In the neutral Mo_2S_7, the bridging disulfide (S_2^{2-}) ligand appears. The Gibbs free energy difference (ΔG) is predicted to be –0.94 kcal mol^{-1}, which should correspond to the removal of S atom from the bridging disulfide S_2^{2-} moiety in Mo_2S_7. As regards its anion and $Mo_2S_8^-$, the S atoms from terminal S_2^{2-} and terminal S_2^- units are removed in the reaction (Eq. 1; n = 7, 8), respectively. The corresponding ΔG is estimated to be –12.51 kcal mol^{-1} (S_2^{2-} for $Mo_2S_7^-$) and –14.74 kcal mol^{-1} (S_2^- for $Mo_2S_8^-$), respectively. Generally, the driving forces ($-\Delta G$) that remove a sulfur atom from various S ligands in $Mo_2S_n^{-/0}$ (n = 4∼8) clusters can be sorted in the order: t–S^{2-} < b–S_2^{2-} < t–S_2^{2-} < t–S_2^-, which in turn stand for the terminal S atom, bridging (μ_2-η^1:η^1) S_2^{2-}, terminal (η^2) S_2^{2-} and terminal (η^2) S_2^- unit, respectively. It seems that the S_2^- units are more reactive with H_2 which would take a S atom away in the form of releasing H_2S molecule. Coordination unsaturated sites (CUS) can be obtained by removing sulfur atoms from the edges of MoS_2 catalyst under the H_2 atmosphere[67]. The order may provide insight into the the pretreatment of fresh MoS_2 catalysts under hydrogen conditions.

5 CONCLUSION

We report a systematical theoretical study on a range of dinuclear metal sulfide clusters: $Mo_2S_n^-$ and Mo_2S_n (n = 4∼8). DFT and CCSD(T) calculations were carried out to elucidate the chemical bonding and geometric and electronic properties of $Mo_2S_n^{-/0}$ clusters. The calculations showed that the sulfur atoms tended to occupy the terminal sites of the clusters continuously in the process of sequential sulfidation. After the oxidation state of Mo atoms gets the maximum of +6, diverse disulfur ligands emerged in the sulfur-rich $Mo_2S_n^{-/0}$ (n = 7, 8) clusters. Additionally, by means of calculating the free energy differences (ΔG) of the reaction (eq. 1), we found that the values of ΔG were positive for the sulfur-deficient and stoichiometric clusters (eq. 2; n = 5, 6), but negative for the sulfur-rich species (Eq. 2; n = 7, 8). The driving forces ($-\Delta G$) for the reactions eliminating sulfur from diverse S ligands in $Mo_2S_n^{-/0}$ (n = 4∼8) clusters followed the general order t–S^{2-} < b–S_2^{2-} < t–S_2^{2-} < t–S_2^-. This order may provide insight into the pretreatment of fresh MoS_2 catalysts under H_2 atmosphere.

REFERENCES

(1) Rapoport, L.; Moshkovich, A.; Perfilyev, V.; Laikhtman, A.; Lapsker, I.; Yadgarov, L.; Rosentsveig, R.; Tenne, R. High lubricity of Re-doped fullerene-like MoS_2 nanoparticles. *Tribol. Lett.* **2012**, 45, 257–264.

(2) Ye, L. N.; Wu, C. Z.; Guo, W.; Xie, Y. MoS_2 hierarchical hollow cubic cages assembled by bilayers: one-step synthesis and their electrochemical hydrogen storage properties. *Chem. Commun*. **2006**, 45, 4738–4740.

(3) Walter, M. G.; Warren, E. L.; McKone, J. R.; Boettcher, S. W.; Mi, Q. X.; Santori, E. A.; Lewis, N. S. Solar water splitting cells. *Chem. Rev*. **2010**, 110, 6446–6473.

(4) Kisielowski, C.; Ramasse, Q. M.; Hansen, L. P.; Brorson, M.; Carlsson, A.; Molenbroek, A. M.; Topsøe, H.; Helveg, S. Imaging MoS_2 nanocatalysts with single-atom sensitivity. *Angew. Chem. Int. Ed*. **2010**, 49, 2708–2710.

(5) Jaramillo, T. F.; Jørgensen, K. P.; Bonde, J.; Nielsen, J. H.; Horch, S.; Chorkendorff, I. Identification of active edge sites for electrochemical H_2 evolution from MoS_2 nanocatalysts. *Science* **2007**, 317, 100–102.

(6) Vajda, S.; White, M. G. Catalysis applications of size-selected cluster deposition. *ACS Catal.* **2015**, 5, 7152–7176.

(7) Deng, Y.; Ting, L. R. L.; Neo, P. H. L.; Zhang, Y. J.; Peterson, A. A.; Yeo, B. S. Operando Raman spectroscopy of amorphous molybdenum sulfide (MoS_x) during the electrochemical hydrogen evolution reaction: identification of sulfur atoms as catalytically active sites for H^+ reduction. *ACS Catal*. **2016**, 6, 7790–7798.

(8) Truong, Q. D.; Devaraju, M. K.; Nguyen, D. N.; Gambe, Y.; Nayuki, K.; Sasaki, Y.; Tran, P. D.; Honma, I. Disulfide-bridged (Mo_3S_{11}) cluster polymer: molecular dynamics and application as electrode material for a rechargeable magnesium battery. *Nano. Lett*. **2016**, 16, 5829–5835.

(9) Kokko, M.; Bayerköhler, F.; Erben, J.; Zengerle, R.; Kurz, P.; Kerzenmacher, S. Molybdenum sulphides on carbon supports as electrocatalysts for hydrogen evolution in acidic industrial wastewater. *Appl. Energ.* **2017**, 190, 1221–1233.

(10) Seger, B.; Herbst, K.; Pedersen, T.; Abrams, B.; Vesborg, P. C. K.; Hansen, O.; Chorkendorff, I. Mo_3S_4 clusters as an effective H_2 evolution catalyst on protected Si photocathodes. *J. Electrochem. Soc.* **2014**, 161, H722–H724.

(11) Vrubel, H.; Merki, D.; Hu, X. Hydrogen evolution catalyzed by MoS_3 and MoS_2 particles. *Energy Environ. Sci*. **2012**, 5, 6136–6144.

(12) Lau, V. W. H.; Masters, A. F.; Bond, A. M.; Maschmeyer, T. Ionic-liquid-mediated active-site control of MoS_2 for the electrocatalytic hydrogen evolution reaction. *Chem. Eur. J*. **2012**, 18, 8230–8239.

(13) Guo, X. N.; Tong, X. L.; Wang, Y. W.; Chen, C. M.; Jin, G. Q.; Guo, X. Y. High photoelectrocatalytic performance of a MoS_2–SiC hybrid structure for hydrogen evolution reaction. *J. Mater. Chem. A* **2013**, 1, 4657–4661.

(14) Liao, L.; Zhu, J.; Bian, X. J.; Zhu, L. N.; Scanlon, M. D.; Girault, H. H.; Liu, B. H. MoS_2 formed on mesoporous graphene as a highly active catalyst for hydrogen evolution. *Adv. Funct. Mater.* **2013**, 23, 5326–5333.

(15) Gary, J. H.; Handwerk, G. E.; Kaiser, M. J. *Petroleum Refining: Technology and Economics, 5th Edition*. CRC Press: Boca Raton, Florida **2007**.

(16) Liu, D.; Li, Z.; Sun, Q.; Kong, X.; Zhao, A. Z.; Wang, Z. X. *In situ* FT-IR study of thiophene adsorbed on the surface of sulfided Mo catalysts. *Fuel* **2012**, 92, 77–83.

(17) Ramos, M.; Berhault, G.; Ferrer, D. A.; Torres, B.; Chianelli, R. R. HRTEM and molecular modeling of the MoS_2–Co_9S_8 interface: understanding the promotion effect in bulk HDS catalysts. *Catal. Sci. Technol.* **2012**, 2, 164–178.

(18) Vogelaar, B. M.; Kagami, N.; van der Zijden, T. F.; van Langeveld, A. D.; Eijsbouts, S.; Moulijn, J. A. Relation between sulfur coordination of active sites and HDS activity for Mo and NiMo catalysts. *J. Mol. Catal. A: Chem.* **2009**, 309, 79–88.

(19) Lauritsen, J. V.; Bollinger, M. V.; Lægsgaard, E.; Jacobsen, K. W.; Nørskov, J. K.; Clausen, B. S.; Topsøe, H.; Besenbacher, F. Atomic-scale insight into structure and morphology changes of MoS_2 nanoclusters in hydrotreating catalysts. *J. Catal*. **2004**, 221, 510–522.

(20) Topsøe, H.; Hinnemann, B.; Nørskov, J. K.; Lauritsen, J. V.; Besenbacher, F.; Hansen, P. L.; Hytoft, G.; Egeberg, R. G.; Knudsen, K. G. The role of reaction pathways and support interactions in the development of high activity hydrotreating catalysts. *Catal. Today* **2005**, 107-108, 12–22.

(21) Vogelaar, B. M.; Steiner, P.; van der Zijden, T. F.; van Langeveld, A. D.; Eijsbouts, S.; Moulijn, J. A. Catalyst deactivation during thiophene HDS: the role of structural sulfur. *Appl. Catal. A: Gen.* **2007**, 318, 28–36.

(22) Besenbacher, F.; Brorson, M.; Clausen, B. S.; Helveg, S.; Hinnemann, B.; Kibsgaard, J.; Lauritsen, J. V.; Moses, P. G.; Nørskov, J. K.; Topsøe, H. Recent STM, DFT and HAADF-STEM studies of sulfide-based hydrotreating catalysts: insight into mechanistic, structural and particle size effects. *Catal. Today* **2008**, 130, 86–96.

(23) Moses, P. G.; Hinnemann, B.; Topsøe, H.; Nørskov, J. K. The effect of copromotion on MoS_2 catalysts for hydrodesulfurization of thiophene: a density functional study. *J. Catal.* **2009**, 268, 201–208.

(24) Joshi, Y. V.; Ghosh, P.; Venkataraman, P. S.; Delgass, W. N.; Thomson, K. T. Electronic descriptors for the adsorption energies of sulfur-containing molecules on Co/MoS_2, using DFT calculations. *J. Phys. Chem. C* **2009**, 113, 9698–9709.

(25) Joshi, Y. V.; Ghosh, P.; Daage, M.; Delgass, W. N. Support effects in HDS catalysts: DFT analysis of thiolysis and hydrolysis energies of metal-support linkages. *J. Catal.* **2008**, 257, 71–80.

(26) Travert, A.; Nakamura, H.; van Santen, R. A.; Cristol, S.; Paul, J. F.; Payen, E. Hydrogen activation on Mo-based sulfide catalysts, a periodic DFT study. *J. Am. Chem. Soc.* **2002**, 124, 7084–7095.

(27) Topsøe, H.; Clausen, B. S.; Massoth, F. E. *Hydrotreating Catalysis in Catalysis-science and Technology*. Anderson, J. R.; Boudart, M. (eds.), 1st Edition; Springer-Verlag Berlin Heidelberg: New York **1996**.

(28) Karunadasa, H. I.; Montalvo, E.; Sun, Y. J.; Majda, M.; Long, J. R.; Chang, C. J. A molecular MoS_2 edge site mimic for catalytic hydrogen generation. *Science* **2012**, 335, 698-702.

(29) Kibsgaard, J.; Jaramillo, T. F.; Besenbacher, F. Building an appropriate active-site motif into a hydrogen-evolution catalyst with thiomolybdate $[Mo_3S_{13}]^{2-}$ clusters. *Nat. Chem.* **2014**, 6, 248–253.

(30) Huang, Z. J.; Luo, W. J.; Ma, L.; Yu, M. Z.; Ren, X. D.; He, M. F.; Polen, S.; Click, K.; Garrett, B.; Lu, J.; Amine, K.; Hadad, C.; Chen, W. L.; Asthagiri, A.; Wu, Y. Y. Dimeric $[Mo_2S_{12}]^{2-}$ cluster: a molecular analogue of MoS_2 edges for superior hydrogen-evolution electrocatalysis. *Angew. Chem. Int. Ed.* **2015**, 54, 15181–15185.

(31) Garrett, B. R.; Polen, S. M.; Click, K. A.; He, M.; Huang, Z.; Hadad, C. M.; Wu, Y. Tunable molecular MoS_2 edge-site mimics for catalytic hydrogen production. *Inorg. Chem.* **2016**, 55, 3960–3966.

(32) Hadjikyriacou, A. I.; Coucouvanis, D. New members of the $[Mo_2(S)_n(S_2)_{6-n}]^{2-}$ series - synthesis, structural characterization, and properties of the $[Mo_2S_9]^{2-}$, $[Mo_2S_7]^{2-}$, and $[Mo_2S_6]^{2-}$ thio anions. *Inorg. Chem.* **1987**, 26, 2400–2408.

(33) Pan, W. H.; Harmer, M. A.; Halbert, T. R.; Stiefel, E. I. Induced internal redox processes in molybdenum-sulfur chemistry - conversion of MoS_4^{2-} to $Mo_2S_8^{2-}$ by organic disulfides. *J. Am. Chem. Soc.* **1984**, 106, 459–460.

(34) Clegg, W.; Christou, G.; Garner, C. D.; Sheldrick, G. M. $[Mo_2S_{10}]^{2-}$, a complex with terminal sulfido, bridging sulfido, persuldido, and tetrasulfido groups. *Inorg. Chem.* **1981**, 20, 1562–1566.

(35) Pan, W. H.; Leonowicz, M. E.; Stiefel, E. I. Facile syntheses of new molybdenum and tungsten sulfido complexes. structure of $Mo_3S_9^{2-}$. *Inorg. Chem.* **1983**, 22, 672–678.

(36) Elder, R. C.; Trkula, M. Crystal structure of $[(NH_3)_5RuSSRu(NH_3)_5]Cl_4{\cdot}2H_2O$. A structural *trans* effect and evidence for a supersulfide S_2^- bridge. *Inorg. Chem.* **1977**, 16, 1048–1051.

(37) York, J. T.; Brown, E. C.; Tolman, W. B. Characterization of a complex comprising a $\{Cu_2(S_2)_2\}^{2+}$ core: bis(μ-S_2^{2-})dicopper(III) or bis(μ-$S_2^{\cdot-}$)dicopper(II)? *Angew. Chem. Int. Ed.* **2005**, 44, 7745–7748.

(38) Yao, S.; Milsmann, C.; Bill, E.; Wieghardt, K.; Driess, M. From a paramagnetic, mononuclear supersulfidonickel(II) complex to a diamagnetic dimer with a four-sulfur two-electron bond. *J. Am. Chem. Soc.* **2008**, 130, 13536–13537.

(39) Yao, S.; Xiong, Y.; Zhang, X.; Schlangen, M.; Schwarz, H.; Milsmann, C.; Driess, M. Facile dissociation of $[(LNi^{II})_2E_2]$ dichalcogenides: evidence for $[LNi^{II}E_2]$ superselenides and supertellurides in solution. *Angew. Chem. Int. Ed.* **2009**, 48, 4551–4554.

(40) Camp, C.; Antunes, M. A.; Garcá, G.; Ciofini, I.; Santos, I. C.; Pécaut, J.; Almeida, M.; Marçalo, J.; Mazzanti, M. Two-electron versus one-electron reduction of chalcogens by uranium(III): synthesis of a terminal U(V) persulfide complex. *Chem. Sci.* **2014**, 5, 841–846.

(41) Johnson, G. E.; Tyo, E. C.; Castleman, A. W. Jr. Cluster reactivity experiments: employing mass spectrometry to investigate the molecular level details of catalytic oxidation reactions. *Proc. Natl. Acad. Sci. USA* **2008**, 105, 18108–18113.

(42) Waters, T.; Huang, X.; Wang, X. B.; Woo, H. K.; O'Hair, R. A. J.; Wedd, A. G.; Wang, L. S. Photoelectron spectroscopy of free multiply charged Keggin anions α-$[PM_{12}O_{40}]^{3-}$ (M = Mo, W) in the gas phase. *J. Phys. Chem. A* **2006**, 110, 10737–10741.

(43) Böhme, D. K.; Schwarz, H. Gas-phase catalysis by atomic and cluster metal ions: the ultimate single-site catalysts. *Angew. Chem., Int. Ed.* **2005**, 44, 2336–2354.

(44) Castleman, A. W. Jr. Cluster structure and reactions: gaining insights into catalytic processes. *Catal. Lett.* **2011**, 141, 1243–1253.

(45) Kumar, C. A.; Saha, A.; Raghavachari, K. Bond activation and hydrogen evolution from water through reactions with M_3S_4 (M = Mo, W) and W_3S_3 anionic clusters. *J. Phys. Chem. A* **2017**, 121, 1760–1767.

(46) Castleman, A. W. Jr.; Jena, P. Clusters: a bridge between disciplines. *Proc. Natl. Acad. Sci. USA* **2006**, 103, 10552–10553.

(47) Murugan, P.; Kumar, V.; Kawazoe, Y.; Ota, N. Atomic structures and magnetism in small MoS_2 and WS_2 clusters. *Phys. Rev. A* **2005**, 71, 063203–6.

(48) Murugan, P.; Kumar, V.; Kawazoe, Y.; Ota, N. Bonding nature and magnetism in small MoX_2 (X = O and S) clusters – a comparative study by first principles calculations. *Chem. Phys. Lett.* **2006**, 423, 202–207.

(49) Patterson, M. J.; Lightstone, J. M.; White, M. G. Structure of molybdenum and tungsten sulfide $M_xS_y^+$ clusters: experiment and DFT calculations. *J. Phys. Chem. A* **2008**, 112, 12011–12021.

(50) Zhou, J.; Zhou, J.; Camillone, N.; White, M. G. Electronic charging of non-metallic clusters: size-selected Mo_xS_y clusters supported on an ultrathin alumina film on NiAl(110). *Phys. Chem. Chem. Phys.* **2012**, 14, 8105–8110.

(51) Bertram, N.; Kim, Y. D.; Ganteför, G.; Sun, Q.; Jena, P.; Tamuliene, J.; Seifert, G. Experimental and theoretical studies on inorganic magic clusters: M_4X_6 (M = W, Mo, X = O, S). *Chem. Phys. Lett.* **2004**, 396, 341–345.

(52) Llusar, R.; Polo, V.; Velez, E.; Vicent, C. Sulfur-based redox reactions in $Mo_3S_7^{4+}$ and $Mo_3S_4^{4+}$ clusters bearing halide and 1,2-dithiolene ligands: a mass spectrometric and density functional theory study. *Inorg. Chem.* **2010**, 49, 8045–8055.

(53) Gemming, S.; Seifert, G.; Götz, M.; Fischer, T.; Ganteför, G. Transition metal sulfide clusters below the cluster-platelet transition: theory and experiment. *Phys. Status Solidi B* **2010**, 247, 1069–1076.

(54) Jiao, H. J.; Li, Y. W.; Delmon, B.; Halet, J. F. The structure and possible catalytic sites of Mo_3S_9 as a model of amorphous molybdenum trisulfide: a computational study. *J. Am. Chem. Soc.* **2001**, 123, 7334–7339.

(55) Mayhall, N. J.; Becher, E. L. III.; Chowdhury, A.; Raghavachari, K. Molybdenum oxides versus molybdenum sulfides: geometric and electronic structures of $Mo_3X_y^-$ (X = O, S and y = 6, 9) clusters. *J. Phys. Chem. A* **2011**, 115, 2291–2296.

(56) Murugan, P.; Kumar, V.; Kawazoe, Y.; Ota, N. *Ab initio* study of structural stability of Mo-S clusters and size specific stoichiometries of magic clusters. *J. Phys. Chem. A* **2007**, 111, 2778–2782.

(57) Gemming, S.; Seifert, G.; Bertram, N.; Fischer, T.; Götz, M.; Ganteför, G. One-dimensional $(Mo_3S_3)_n$ clusters: building blocks of clusters materials and ideal nanowires for molecular electronics. *Chem. Phys. Lett.* **2009**, 474, 127–131.

(58) Gemming, S.; Tamuliene, J.; Seifert, G.; Bertram, N.; Kim, Y. D.; Ganteför, G. Electronic and geometric structures of Mo_xS_y and W_xS_y (x = 1, 2, 4; y = 1～12) clusters. *Appl. Phys. A* **2006**, 82, 161–166.

(59) Liang, B. Y.; Andrews, L. Infrared spectra and density functional theory calculations of group 6 transition metal sulfides in solid argon. *J. Phys. Chem. A* **2002**, 106, 6945–6951.

(60) Pietsch, S.; Dollinger, A.; Strobel, C. H.; Park, E. J.; Gantefor, G.; Seo, H. O.; Kim, Y. D.; Idrobo J. C.; Pennycook, S. J. The quest for inorganic fullerenes. *J. Appl. Phys.* **2015**, 118, 134302–7.

(61) Wang, B.; Wu, N.; Zhang, X. B.; Huang, X.; Zhang, Y. F.; Chen, W. K.; Ding, K. N. Probing the smallest molecular model of MoS_2 catalyst: S_2 units in the $MoS_n^{-/0}$ (n = 1～5) clusters. *J. Phys. Chem. A* **2013**, 117, 5632–5641.

(62) Wu, N.; Zhang, C. F.; Zhou, Q.; Huang, X.; Zhang, Y. F.; Ding, K. N.; Wang, B. DFT study on the electronic and structural properties of $MoS_6^{-/0}$ clusters. *Chin. J. Struc. Chem.* **2013**, 32, 1046–1054.

(63) Wang, B.; Chen, W. J.; Zhao, B. C.; Zhang, Y. F.; Huang, X. Tetratungsten oxide clusters $W_4O_n^{-/0}$ (n = 10～13): structural evolution and chemical bonding. *J. Phys. Chem. A* **2010**, 114, 1964–1972.

(64) Zhai, H. J.; Wang, B.; Huang, X.; Wang, L. S. Probing the electronic and structural properties of the niobium trimer cluster and its mono- and dioxides: $Nb_3O_n^-$ and Nb_3O_n (n = 0～2). *J. Phys. Chem. A* **2009**, 113, 3866–3875.

(65) Zhai, H. J.; Wang, B.; Huang, X.; Wang, L. S. Structural evolution, sequential oxidation, and chemical bonding in tritantalum oxide clusters: $Ta_3O_n^-$ and Ta_3O_n (n = 1～8). *J. Phys. Chem. A* **2009**, 113, 9804–9813.

(66) Wang, B.; Zhai, H. J.; Huang, X.; Wang, L. S. On the electronic structure and chemical bonding in the tantalum trimer cluster. *J. Phys. Chem. A* **2008**, 112, 10962–10967.

(67) Afanasiev, P. The influence of reducing and sulfiding conditions on the properties of unsupported MoS_2–based catalysts. *J. Catal.* **2010**, 269, 269–280.

(68) Afanasiev, P.; Jobic, H.; Lorentz, C.; Leverd, P.; Mastubayashi, N.; Piccolo, L.; Vrinat, M. Low-temperature hydrogen interaction with amorphous molybdenum sulfides MoS_x. *J. Phys. Chem. C* **2009**, 113, 4139–4146.

(69) Duchet, J.; Van Oers, E.; De Beer, V.; Prins, R. Carbon-supported sulfide catalysts. *J. Catal.* **1983**, 80, 386–402.

(70) Becke, A. D. A new mixing of hartree-fock and local density-functional theories. *J. Chem. Phys.* **1993**, 98, 1372–1377.

(71) Lee, C.; Yang, W.; Parr, R. G. Development of the colle-salvetti correlation-energy formula into a functional of the electron density. *Phys. Rev. B* **1988**, 37, 785–789.

(72) Stephens, P. J.; Devlin, F. J.; Chabalowski, C. F.; Frisch, M. J. *Ab initio* calculation of vibrational absorption and circular dichroism spectra using density functional force fields. *J. Phys. Chem.* **1994**, 98, 11623–11627.

(73) Frisch, M. J.; Trucks, G. W.; Schlegel, H. B.; Scuseria, G. E.; Robb, M. A.; Cheeseman, J. R.; Montgomery, J. A. Jr.; Vreven, T.; Kudin, K. N.; Burant, J. C.; Millam, J. M.; Iyengar, S. S.; Tomasi, J.; Barone, V.; Mennucci, B.; Cossi, M.; Scalmani, G.; Rega, N.; Petersson, G. A.; Nakatsuji, H.; Hada, M.; Ehara, M.; Toyota, K.; Fukuda, R.; Hasegawa, J.; Ishida, M.; Nakajima, T.; Honda, Y.; Kitao, O.; Nakai, H.; Klene, M.; Li, X.; Knox, J. E.; Hratchian, H. P.; Cross, J. B.; Bakken, V.; Adamo, C.; Jaramillo, J.; Gomperts, R.; Stratmann, R. E.; Yazyev, O.; Austin, A. J.; Cammi, R.; Pomelli,

C.; Ochterski, J. W.; Ayala, P. Y.; Morokuma, K.; Voth, G. A.; Salvador, P.; Dannenberg, J. J.; Zakrzewski, V. G.; Dapprich, S.; Daniels, A. D.; Strain, M. C.; Farkas, O.; Malick, D. K.; Rabuck, A. D.; Raghavachari, K.; Foresman, J. B.; Ortiz, J. V.; Cui, Q.; Baboul, A. G.; Clifford, S.; Cioslowski, J.; Stefanov, B. B.; Liu, G.; Liashenko, A.; Piskorz, P.; Komaromi, I.; Martin, R. L.; Fox, D. J.; Keith, T.; Al-Laham, M. A.; Peng, C. Y.; Nanayakkara, A.; Challacombe, M.; Gill, P. M. W.; Johnson, B.; Chen, W.; Wong, M. W.; Gonzalez, C.; Pople, J. A. *Gaussian 03*; *Revision D.01*; Gaussian, Inc.: Wallingford, CT **2004**.

(74) Sousa, S. F.; Fernandes, P. A.; Ramos, M. J. General performance of density functionals. *J. Phys. Chem. A* **2007**, 111, 10439−10452.

(75) Schäfer, A.; Huber, C.; Ahlrichs, R. Fully optimized contracted Gaussian basis sets of triple zeta valence quality for atoms Li to Kr. *J. Chem. Phys.* **1994**, 100, 5829−5835.

(76) Weigend, F.; Ahlrichs, R. Balanced basis sets of split valence, triple zeta valence and quadruple zeta valence quality for H to Rn: design and assessment of accuracy. *Phys. Chem. Chem. Phys.* **2005**, 7, 3297−3305.

(77) Eichkorn, K.; Weigend, F.; Treutler, O.; Ahlrichs, R. Auxiliary basis sets for main row atoms and transition metals and their use to approximate coulomb potentials. *Theor. Chem. Acc.* **1997**, 97, 119−124.

(78) Andrae, D.; Haeussermann, U.; Dolg, M.; Stoll, H.; Preuss, H. Energy-adjusted *ab initio* pseudopotentials for the second and third row transition elements. *Theor. Chim. Acta* **1990**, 77, 123−141.

(79) Küchle, W.; Dolg, M.; Stoll, H.; Preuss, H. *Pseudopotentials of the Stuttgart/Dresden Group 1998*, revision August 11 **1998**; http://www.theochem.uni-stuttgart.de/pseudopotentiale.

(80) Martin, J. M. L.; Sundermann, A. Correlation consistent valence basis sets for use with the Stuttgart-dresden-bonn relativistic effective core potentials: the atoms Ga-Kr and In-Xe. *J. Chem. Phys.* **2001**, 114, 3408−3420.

(81) Dunning, T. H. Jr. Gaussian basis sets for use in correlated molecular calculations. I. the atoms boron through neon and hydrogen. *J. Chem. Phys.* **1989**, 90, 1007−1023.

(82) Woon, D. E.; Dunning, T. H. Jr. Gaussian basis sets for use in correlated molecular calculations. III. The atoms aluminum through argon. *J. Chem. Phys.* **1993**, 98, 1358−1371.

(83) Dunning, T. H.; Peterson, K. A.; Wilson, A. K. Gaussian basis sets for use in correlated molecular calculations. X. the atoms aluminum through argon revisited. *J. Chem. Phys.* **2001**, 114, 9244−9253.

(84) Purvis, G. D. III; Bartlett, R. J. A full coupled-cluster singles and doubles model: the inclusion of disconnected triples. *J. Chem. Phys.* **1982**, 76, 1910−1918.

(85) Scuseria, G. E.; Janssen, C. L.; Schaefer, H. F. III. An efficient reformulation of the closed-shell coupled cluster single and double excitation (CCSD) equations. *J. Chem. Phys.* **1988**, 89, 7382−7387.

(86) Raghavachari, K.; Trucks, G. W.; Pople, J. A.; Head-Gordon, M. A 5th-order perturbation comparison of electron correlation theories. *Chem. Phys. Lett.* **1989**, 157, 479−483.

(87) Watts, J. D.; Gauss, J.; Bartlett, R. J. Coupled-cluster methods with noniterative triple excitations for restricted open-shell hartree-fock and other general single determinant reference functions - energies and analytical gradients. *J. Chem. Phys.* **1993**, 98, 8718−8733.

(88) Bartlett, R. J.; Musial, M. Coupled-cluster theory in quantum chemistry. *Rev. Mod. Phys.* **2007**, 79, 291−352.

(89) Tozer, D. J.; Handy, N. C. Improving virtual Kohn-Sham orbitals and eigenvalues: application to excitation energies and static polarizabilities. *J. Chem. Phys.* **1998**, 109, 10180−10189.

(90) Werner, H. J.; Knowles, P. J.; Manby, F. R.; Schütz, M.; Celani, P.; Knizia, G.; Korona, T.; Lindh, R.; Mitrushenkov, A.; Rauhut, G.; Adler, T. B.; Amos, R. D.; Bernhardsson, A.; Berning, A.; Cooper, D. L.; Deegan, M. J. O.; Dobbyn, A. J.; Eckert, F.; Goll, E.; Hampel, C.; Hesselmann, A.; Hetzer, G.; Hrenar, T.; Jansen, G.; Köppl, C.; Liu, Y.; Lloyd, A. W.; Mata, R. A.; May, A. J.; McNicholas, S. J.; Meyer, W.; Mura, M. E.; Nicklass, A.; O'Neill, D. P.; Palmieri, P.; Pflüger, K.; Pitzer, R.; Reiher, M.; Shiozaki, T.; Stoll, H.; Stone, A. J.; Tarroni, R.; Thorsteinsson, T.; Wang, M.; Wolf, A. *MOLPRO*, version 2010.1, a package of ab initio programs; see http://www.molpro.net.

(91) Humphrey, W.; Dalke, A.; Schulten, K. VMD: visual molecular dynamics. *J. Mol. Graphics.* **1996**, 14, 33−38.

(92) Rienstra-Kiracofe, J. C.; Tschumper, G. S.; Schaefer, H. F. III.; Nandi, S.; Ellison, G. B. Atomic and molecular electron affinities: photoelectron experiments and theoretical computations. *Chem. Rev.* **2002**, 102, 231−282.

(93) Ganteför, G. *Photoelectron Spectroscopy. In Quantum Phenomena in Clusters and Nanostructures. Series: Springer Series in Cluster Physics.* Khanna, S. N.; Castleman, A. W. Jr. (Eds.), 1st Edition; Springer-Verlag Berlin Heidelberg: New York **2003**.

(94) Huang, X.; Zhai, H. J.; Kiran, B.; Wang, L. S. Observation of *d*-orbital aromaticity. *Angew. Chem. Int. Ed.* **2005**, 44, 7251−7254.

(95) Xie, L.; Li, W. L.; Romanescu, C.; Huang, X.; Wang, L. S. A photoelectron spectroscopy and density functional study of di-tantalum boride clusters: $Ta_2B_x^-$ (x = 2∼5). *J. Chem. Phys.* **2013**, 138, 034308−11.

(96) Li, H. F.; Kuang, X. Y.; Wang, H. Q. Probing the structural and electronic properties of lanthanide-metal-doped silicon clusters: M@Si-6 (M = Pr, Gd, Ho). *Phys. Lett. A* **2011**, 375, 2836–2844.

Table 1. Relative Energies of the Low-lying Isomers of the $Mo_2S_n^{-/0}$ (n = 4∼8) Clusters at the B3LYP Level (ΔE < 0.40 eV), and Comparisons with Those from the CCSD(T) Single-point Calculations at the B3LYP Geometries

	Electronic state	B3LYP[a, b]	CCSD(T)[a, c]
Mo_2S_4	($C_s{}^3A''$)	**0.00**	0.07
	($C_{2v}{}^3A_2$)	0.04	**0.00**
	($C_{2v}{}^5B_1$)	0.15	0.38
	($C_{2h}{}^5B_g$)	0.21	0.44
	($C_s{}^3A''$)	0.30	0.46
	($C_{2v}{}^1A_1$)	0.39	0.22
$Mo_2S_4^-$	($C_{2v}{}^4B_1$)	**0.00**	**0.00**
	($C_{2h}{}^4B_g$)	0.18	0.17
	($C_{2v}{}^2B_1$)	0.34	0.09
Mo_2S_5	($C_s{}^1A'$)	**0.00**	**0.00**
	($C_s{}^3A'$)	0.17	0.40
$Mo_2S_5^-$	($C_s{}^2A'$)	**0.00**	**0.00**
	($C_{2v}{}^4A_2$)	0.22	0.41
Mo_2S_6	($C_{2v}{}^1A_1$)	**0.00**	---
$Mo_2S_6^-$	($D_{2h}{}^2A_g$)	**0.00**	---
Mo_2S_7	($C_2{}^1A$)	**0.00**	**0.00**
	($C_s{}^3A''$)	0.26	0.40
	($C_1{}^1A$)	0.39	0.45
$Mo_2S_7^-$	($C_1{}^2A$)	**0.00**	**0.00**
	($C_2{}^2A$)	0.39	0.37
Mo_2S_8	($C_{2v}{}^3B_2$)	**0.00**	**0.00**
	($C_{2h}{}^3B_u$)	0.20	0.23
$Mo_2S_8^-$	($C_{2v}{}^2B_1$)	**0.00**	**0.00**
	($C_{2h}{}^2B_g$)	0.06	0.06
	($C_s{}^2A'$)	0.11	0.34

[a] All energies are in eV. [b] B3LYP/H-BS. [c] CCSD(T) single-point calculations at the B3LYP/H-BS geometries

Table 2. Vertical Detachment Energies (VDEs) of the Lowest-energy $Mo_2S_n^{-/0}$ (n = 4～8) Clusters and Selected Low-lying Isomer (ΔE < 0.4 eV) at the B3LYP Level

	MO[b]	VDE[a, b]	MO[b]	VDE[a, b]
$Mo_2S_4^-$	$19a_1(\alpha)$	3.39(Tri)		
(C_{2v} $^4B_1$ 0.00 eV)	$13b_2(\alpha)$	3.46(Tri)		
	$6a_2(\alpha)$	3.63(Tri)		
	$18a_1(\alpha)$	4.51(Tri)	$18a_1(\beta)$	3.59(Qui)
	$10b_1(\alpha)$	4.60(Tri)	$10b_1(\beta)$	4.66(Qui)
	$17a_1(\alpha)$	5.36(Tri)	$17a_1(\beta)$	5.18(Qui)
	$5a_2(\alpha)$	5.39(Tri)	$12b_2(\beta)$	5.23(Qui)
	$12b_2(\alpha)$	5.57(Tri)	$5a_2(\beta)$	5.32(Qui)
	$16a_1(\alpha)$	5.76(Tri)	$16a_1(\beta)$	5.65(Qui)
$Mo_2S_4^-$	$9a_u(\alpha)$	3.31(Tri)		
(C_{2h} ^4B_g 0.18 eV)	$17a_g(\alpha)$	3.32(Tri)		
	$15b_u(\alpha)$	3.81(Tri)		
	$16a_g(\alpha)$	4.34(Tri)	$16a_g(\beta)$	3.30(Qui)
	$7b_g(\alpha)$	5.05(Tri)	$7b_g(\beta)$	4.94(Qui)
	$8a_u(\alpha)$	5.27(Tri)	$8a_u(\beta)$	4.94(Qui)
	$14b_u(\alpha)$	5.45(Tri)	$15a_g(\beta)$	5.22(Qui)
	$15a_g(\alpha)$	5.48(Tri)	$14b_u(\beta)$	5.23(Qui)
	$13b_u(\alpha)$	5.68(Tri)	$13b_u(\beta)$	5.65(Qui)
$Mo_2S_4^-$	$19a_1(\alpha)$	3.32(Sin)		
(C_{2v} $^2B_1$ 0.34 eV)	$11b_1(\alpha)$	3.72(Sin)	$19a_1(\beta)$	3.25(Tri)
	$10b_1(\alpha)$	4.56(Sin)	$10b_1(\beta)$	4.52(Tri)
	$12b_2(\alpha)$	4.90(Sin)	$12b_2(\beta)$	4.90(Tri)
	$5a_2(\alpha)$	5.07(Sin)	$5a_2(\beta)$	5.06(Tri)
	$18a_1(\alpha)$	5.23(Sin)	$18a_1(\beta)$	5.12(Tri)
	$17a_1(\alpha)$	5.43(Sin)	$17a_1(\beta)$	5.36(Tri)
$Mo_2S_5^-$	$38a'(\alpha)$	3.76(Sin)		
(C_s $^2A'$ 0.00 eV)	$37a'(\alpha)$	4.50(Sin)	$37a'(\beta)$	4.03(Tri)
	$36a'(\alpha)$	4.65(Sin)	$36a'(\beta)$	4.50(Tri)
	$17a''(\alpha)$	4.93(Sin)	$17a''(\beta)$	4.93(Tri)
	$16a''(\alpha)$	5.43(Sin)	$16a''(\beta)$	5.43(Tri)
	$35a'(\alpha)$	5.77(Sin)	$35a'(\beta)$	5.65(Tri)
	$34a'(\alpha)$	5.86(Sin)	$34a'(\beta)$	5.84(Tri)
	$15a''(\alpha)$	5.91(Sin)	$15a''(\beta)$	5.88(Tri)
$Mo_2S_5^-$	$5a_2(\alpha)$	3.81(Tri)		
(C_{2v} $^4A_2$ 0.22 eV)	$25a_1(\alpha)$	4.11(Tri)		
	$13b_1(\alpha)$	4.62(Tri)		
	$24a_1(\alpha)$	4.96(Tri)	$13b_1(\beta)$	4.61(Qui)
	$13b_2(\alpha)$	5.22(Tri)	$4a_2(\beta)$	5.21(Qui)
	$12b_1(\alpha)$	5.74(Tri)	$13b_2(\beta)$	5.21(Qui)
	$12b_2(\alpha)$	5.78(Tri)	$12b_2(\beta)$	5.73(Qui)
	$4a_2(\alpha)$	5.93(Tri)	$12b_1(\beta)$	5.77(Qui)
$Mo_2S_6^-$	$15a_g(\alpha)$	4.51(Sin)		
(D_{2h} ^2A_g 0.00 eV)	$10b_{2u}(\alpha)$	4.63(Sin)	$10b_{2u}(\beta)$	4.64(Tri)
	$4b_{3g}(\alpha)$	4.80(Sin)	$4b_{3g}(\beta)$	4.84(Tri)
	$8b_{1g}(\alpha)$	4.92(Sin)	$8b_{1g}(\beta)$	4.94(Tri)
	$8b_{1u}(\alpha)$	5.44(Sin)	$8b_{1u}(\beta)$	5.43(Tri)
	$5b_{2g}(\alpha)$	5.98(Sin)	$5b_{2g}(\beta)$	5.98(Tri)
$Mo_2S_7^-$	$71a(\alpha)$	4.32(Sin)		
(C_1 ^2A 0.00 eV)	$70a(\alpha)$	4.75(Sin)	$70a(\beta)$	4.26(Tri)
	$69a(\alpha)$	4.91(Sin)	$69a(\beta)$	4.81(Tri)
	$68a(\alpha)$	5.00(Sin)	$68a(\beta)$	4.96(Tri)
	$67a(\alpha)$	5.55(Sin)	$67a(\beta)$	5.53(Tri)
	$66a(\alpha)$	5.75(Sin)	$66a(\beta)$	5.76(Tri)
$Mo_2S_7^-$	$37a(\alpha)$	3.53(Sin)		
(C_2 ^2A 0.39 eV)	$34b(\alpha)$	4.72(Sin)	$34b(\beta)$	4.68(Tri)

	36a(α)	5.04(Sin)	33b(β)	4.97(Tri)
	33b(α)	5.06(Sin)	36a(β)	4.99(Tri)
	35a(α)	5.45(Sin)	35a(β)	5.12(Tri)
	34a(α)	5.72(Sin)	34a(β)	5.68(Tri)
	32b(α)	5.91(Sin)	32b(β)	5.89(Tri)
$Mo_2S_8^-$	18b_1(α)	4.42(Sin)		
(C_{2v} $^2B_1$ 0.00 eV)	13a_2(α)	4.49(Sin)	13a_2(β)	3.58(Tri)
	27a_1(α)	4.53(Sin)	27a_1(β)	4.52(Tri)
	17b_1(α)	4.80(Sin)	17b_1(β)	4.61(Tri)
	26a_1(α)	5.38(Sin)	26a_1(β)	5.23(Tri)
	16b_1(α)	5.39(Sin)	16b_1(β)	5.36(Tri)
	21b_2(α)	5.76(Sin)	21b_2(β)	5.70(Tri)
$Mo_2S_8^-$	15b_g(α)	4.36(Sin)		
(C_{2h} ^2B_g 0.06 eV)	25a_g(α)	4.42(Sin)	16a_u(β)	3.73(Tri)
	16a_u(α)	4.61(Sin)	25a_g(β)	4.43(Tri)
	14b_g(α)	4.73(Sin)	14b_g(β)	4.55(Tri)
	23b_u(α)	5.24(Sin)	23b_u(β)	5.07(Tri)
	15a_u(α)	5.38(Sin)	15a_u(β)	5.35(Tri)
	24a_g(α)	5.87(Sin)	24a_g(β)	5.82(Tri)
Mo_2S_8	52a'(α)	4.32(Sin)		
(C_s $^2A'$ 0.11 eV)	51a'(α)	4.63(Sin)	51a'(β)	4.24(Tri)
	27a"(α)	4.69(Sin)	50a'(β)	4.53(Tri)
	50a'(α)	4.74(Sin)	27a"(β)	4.65(Tri)
	26a"(α)	5.37(Sin)	26a"(β)	5.35(Tri)
	25a"(α)	5.75(Sin)	25a"(β)	5.38(Tri)
	49a'(α)	5.83(Sin)	49a'(β)	5.69(Tri)
	48a'(α)	5.98(Sin)	48a'(β)	5.90(Tri)

[a] All energies are in eV.

[b] The labels "α" and "β" denote the majority and minority spins, whereas Sin, Tri and Qui denote the singlet, triplet and quintet $Mo_2S_n^{-/0}$ (n = 4∼8) final states upon photodetachment

Table 3. Calculated Free Energy Differences (Δ*G*) for the Proposed Reaction (Eq. 1) at the B3LYP/H-BS Level of Theory

n→*n*-1	ΔG_{ne} [a, b]	Losing sulfur [c]	ΔG_{an} [a,b]	Losing sulfur [c]
5→4	30.95	t–S^{2-}	39.01	t–S^{2-}
6→5	15.45	t–S^{2-}	32.29	t–S^{2-}
7→6	–0.94	b–S_2^{2-}	–12.51	t–S_2^{2-}
8→7	–7.04	---	–14.74	t–S_2^{-}

[a] All energies are in kcal mol^{-1}.

[b] ΔG_{an} and ΔG_{ne} represent the ΔG of anionic and neutral clusters, respectively.

[c] The labels "t–S^{2-}", "b–S_2^{2-}", "t–S_2^{-}" and "t–S_2^{2-}" denote the sulfur atom losing from the terminal S, bridging (μ_2-η^1:η^1) S_2^{2-}, terminal (η^2) S_2^{-} and terminal (η^2) S_2^{2-} upon the reduction reaction (Eq. 1).

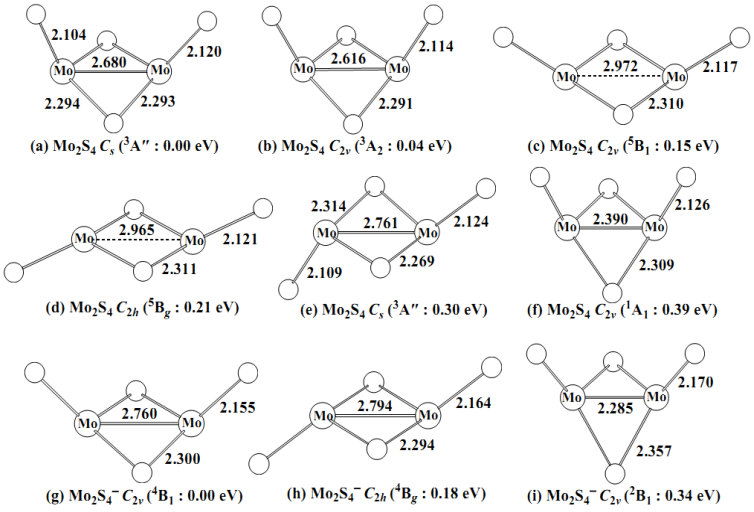

Fig. 1. Optimized structures for Mo_2S_4 and $Mo_2S_4^-$. The bond lengths are in angstroms (Å)

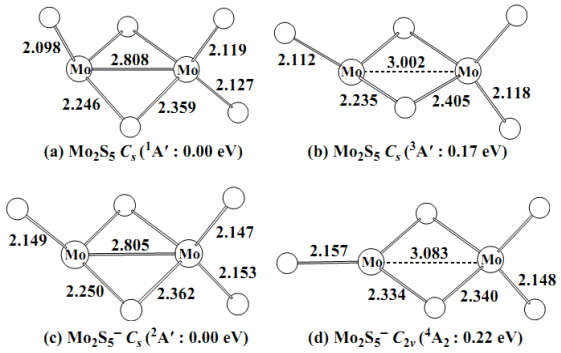

Fig. 2. Optimized structures for Mo_2S_5 and $Mo_2S_5^-$. The bond lengths are in angstroms (Å)

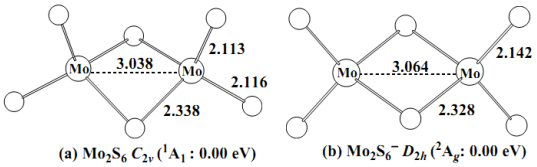

(a) Mo_2S_6 C_{2v} ($^1A_1$: 0.00 eV) (b) $Mo_2S_6^-$ D_{2h} (^2A_g: 0.00 eV)

Fig. 3. Optimized structures for Mo_2S_6 and $Mo_2S_6^-$. The bond lengths are in angstroms (Å)

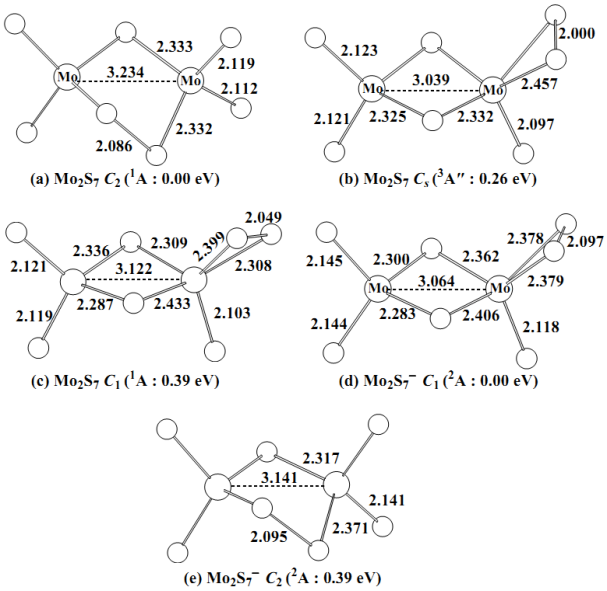

(a) Mo_2S_7 C_2 (^1A : 0.00 eV) (b) Mo_2S_7 C_s ($^3A''$: 0.26 eV)

(c) Mo_2S_7 C_1 (^1A : 0.39 eV) (d) $Mo_2S_7^-$ C_1 (^2A : 0.00 eV)

(e) $Mo_2S_7^-$ C_2 (^2A : 0.39 eV)

Fig. 4. Optimized structures for Mo_2S_7 and $Mo_2S_7^-$. The bond lengths are in angstroms (Å)

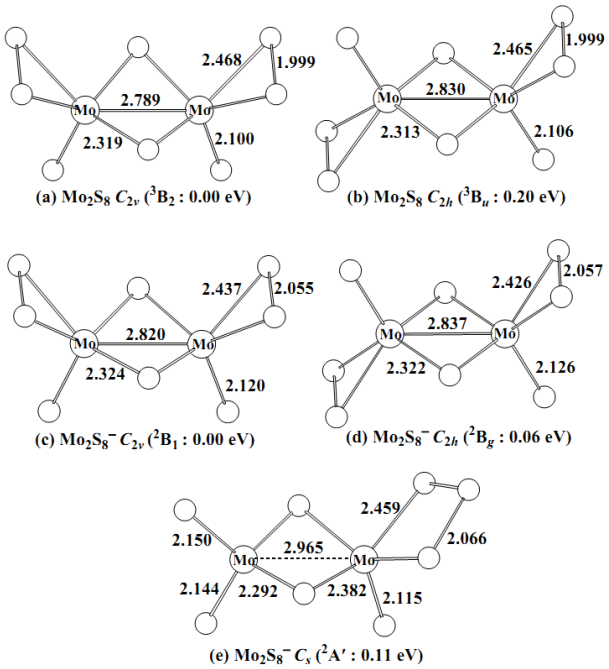

Fig. 5. Optimized structures for Mo_2S_8 and $Mo_2S_8^-$. The bond lengths are in angstroms (Å)

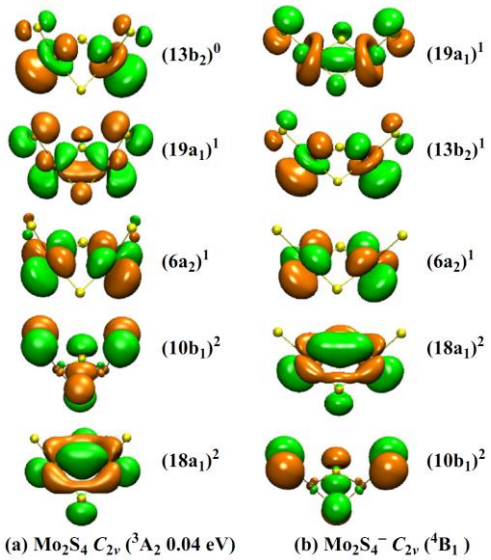

Fig. 6. (a) Frontier molecular orbitals for the neutral Mo_2S_4 ground state (Fig. 1b). (b) Frontier molecular orbitals for the anionic $Mo_2S_4^-$ ground state (Fig. 1g)

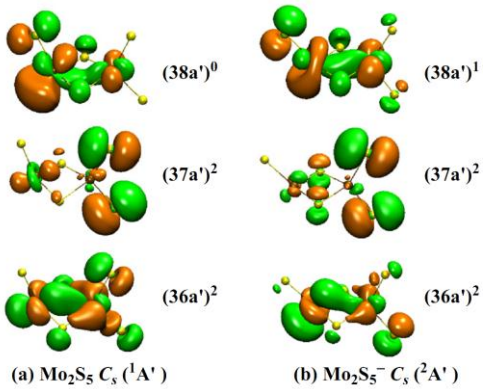

Fig. 7. (a) Frontier molecular orbitals for the neutral Mo_2S_5 ground state (Fig. 2a). (b) Frontier molecular orbitals for the anionic $Mo_2S_5^-$ ground state (Fig. 2c)

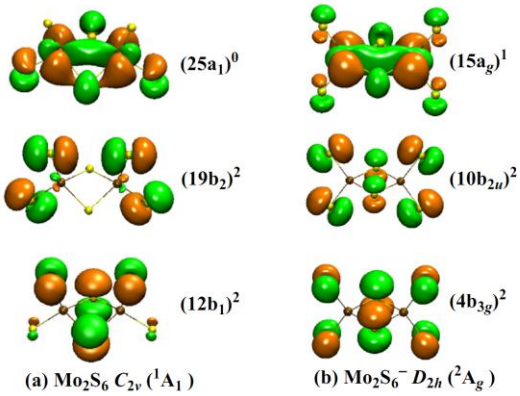

Fig. 8. (a) Frontier molecular orbitals for the neutral Mo_2S_6 ground state (Fig. 3a). (b) Frontier molecular orbitals for the anionic $Mo_2S_6^-$ ground state (Fig. 3b)

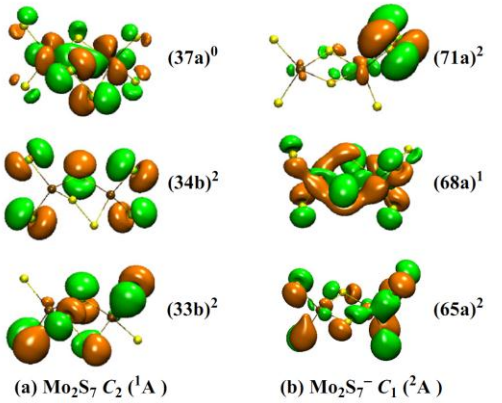

Fig. 9. (a) Frontier molecular orbitals for the neutral Mo_2S_7 ground state (Fig. 4a). (b) Selected frontier molecular orbitals for the anionic $Mo_2S_7^-$ ground state (Fig. 4d)

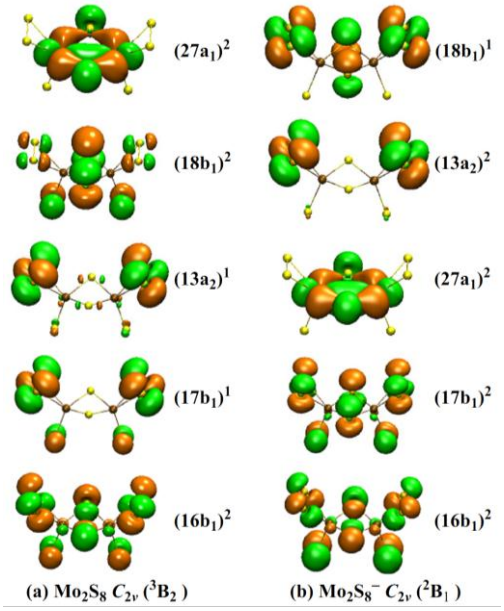

Fig. 10. (a) Selected frontier molecular orbitals for the neutral Mo_2S_8 ground state (Fig. 5a). (b) Selected frontier molecular orbitals for the anionic $Mo_2S_8^-$ ground state (Fig. 5c)

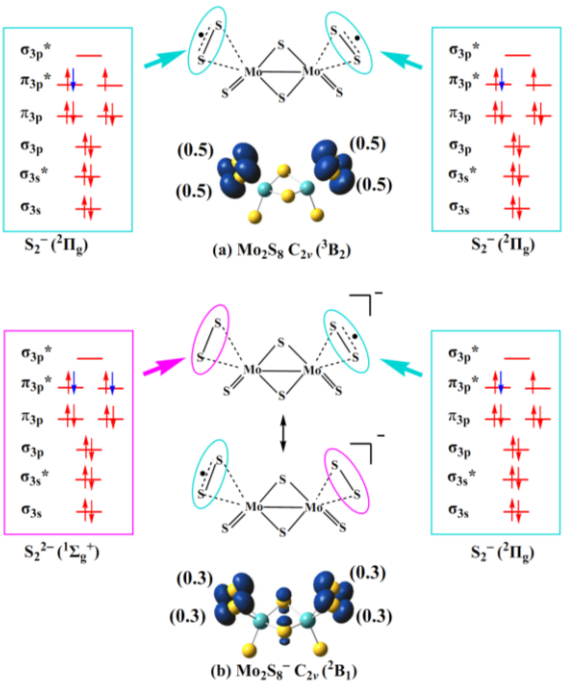

Fig. 11. Valence bond descriptions and numerical electron spin density (in |e|) for the ground state of $Mo_2S_8^{-/0}$ clusters. The numerical spin density was shown in parentheses

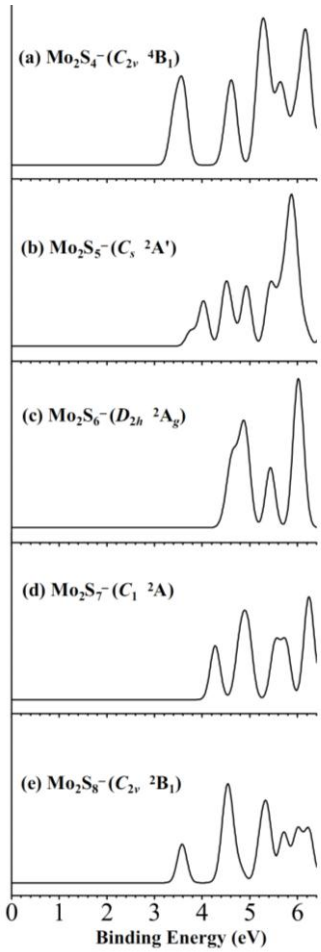

Fig. 12. Simulated photoelectron spectra from the ground states for $Mo_2S_n^-$ (n = 4～8) clusters at the B3LYP/H-BS level. The simulations are done by fitting the distribution of calculated VDEs with unit-area Gaussian functions of 0.1 eV width

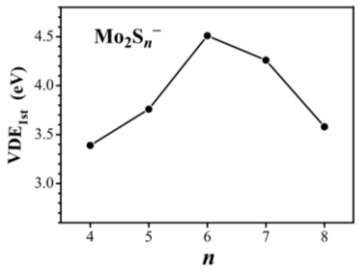

Fig. 13. Calculated first vertical detachment energies (VDE_{1st}) of $Mo_2S_n^-$ (n = 4～8) as a function of S content (n)

Probing Diverse Disulfur Ligands in the $Mo_2S_n^{-/0}$ (n = 4 ～ 8) Clusters: Structural Evolution and Chemical Bonding

ZHANG Xiao-Fei(张晓菲)　LIU Xiu-Juan(刘秀娟)　XU Ruo-Nan(徐若男)

WU Ni(吴妮)　HUANG Xin(黄昕)　WANG Bin(王彬)

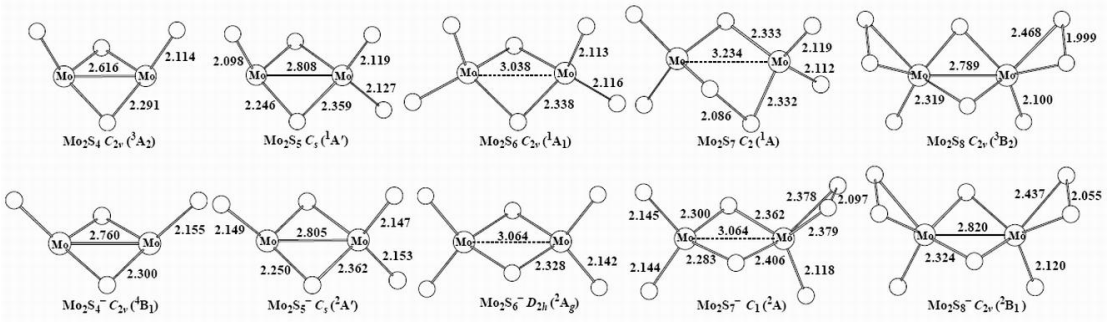

Density functional theory (DFT) and coupled cluster theory (CCSD(T)) calculations were employed to investigate the geometric and electronic structures of a range of dinuclear molybdenum sulfide clusters, $Mo_2S_n^-$ and Mo_2S_n (n = 4～8). After the oxidation state of Mo atoms reached the maximum of +6, diverse disulfur ligands emerged in the sulfur-rich $Mo_2S_n^{-/0}$ (n = 7, 8) clusters. The driving forces of removing a sulfur atom from different S ligands in $Mo_2S_n^{-/0}$ (n = 4～8) clusters, especially from those disulfur units, were evaluated. Vertical detachment energies (VDEs) were predicted, and then the photoelectron spectra (PES) were simulated. Molecular orbital and spin density values were analyzed to elucidate the chemical bonding and the evolutionary behavior in the dinuclear molybdenum sulfide clusters.